New Insights into the Strain Coupling to Surface Chemistry, Electronic Structure and Reactivity of $La_{0.7}Sr_{0.3}MnO_3$

Helia Jalili[1†], Jeong Woo Han[1,2†], Yener Kuru[1,2,3], Zhuhua Cai[1,2], and Bilge Yildiz[1,2*]

[1]*Laboratory for Electrochemical Interfaces,* [2]*Department of Nuclear Science and Engineering,*
[3]*Department of Materials Science and Engineering,*
Massachusetts Institute of Technology, 77 Massachusetts Avenue, Cambridge, MA 02139, USA

Supporting Information Available: 1) X-ray diffraction patterns, 2) Scanning tunneling spectra (STS) taken on $La_{0.7}Sr_{0.3}MnO_3$ films grown on $SrTiO_3$ (STO) and $LaAlO_3$ (LAO); 3) the DFT model construction and description, and 4) the calculated total density of states on LSM(001) that shows a change in the band gap value as a function of strain. This material is available free of charge via the Internet at http://pubs.acs.org

1) LSM crystallographic structure and strain state on STO and LAO.

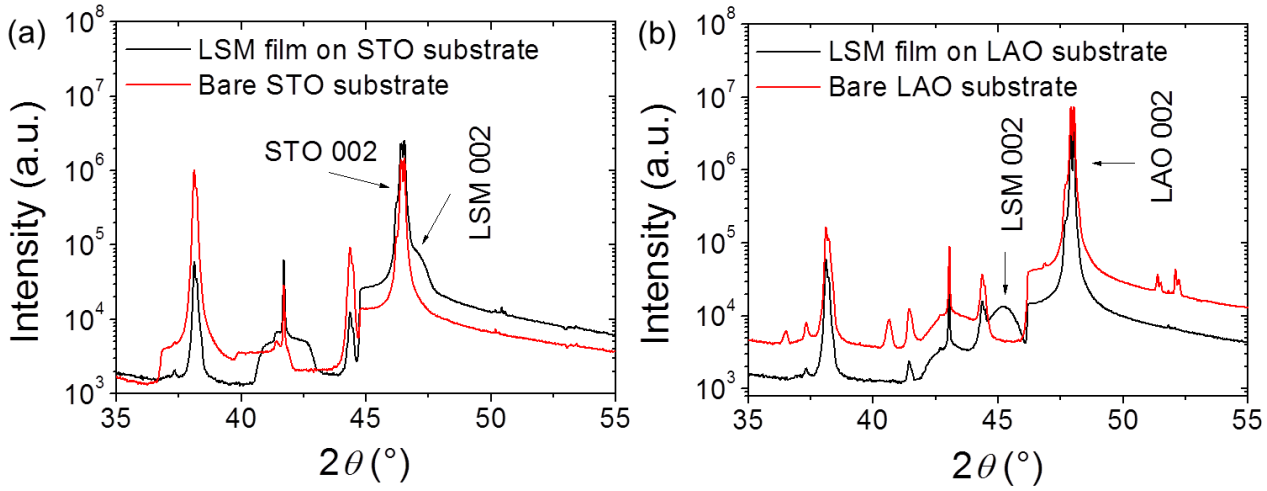

Figure S1: (2θ-ω) scans in logarithmic intensity scale of (a) LSM/LAO (black curve) and LAO bare substrate (red curve) and (b) LSM/STO (black curve) and STO bare substrate (red curve).

We used the c/a ratio reported in a previous report[1] for the LSM film on (001) LAO substrate to convert the out-of-plane lattice parameter (i.e. c-axis) to in-plane lattice parameter (i.e. a-axis).

* To whom correspondence should be addressed. Email: byildiz@mit.edu
†These authors contributed equally to this work.

Compound	Lattice Parameter Å	Thermal expansion coefficient /°C	Lattice mismatch LSM ε(%) at RT	Lattice mismatch LSM ε(%) at 850 °C
[2]$La_{0.7}Sr_{0.3}MnO_3$	3.873	1.28×10^{-5}	0	0
[3]$SrTiO_3$	3.905	1.04×10^{-5}	+0.8	+0.6
[1]$LaAlO_3$	3.790	1.00×10^{-5}	-2.1	-2.3

Table S1: Lattice mismatch between the LSM films and the substrates STO and LAO at room temperature (RT) and at 850 °C. The latter is calculated using the thermal expansion coefficients of LSM, STO and LAO.

2) Tunneling current vs. sample bias on LSM/LAO and LSM/STO at room temperature and at high temperature

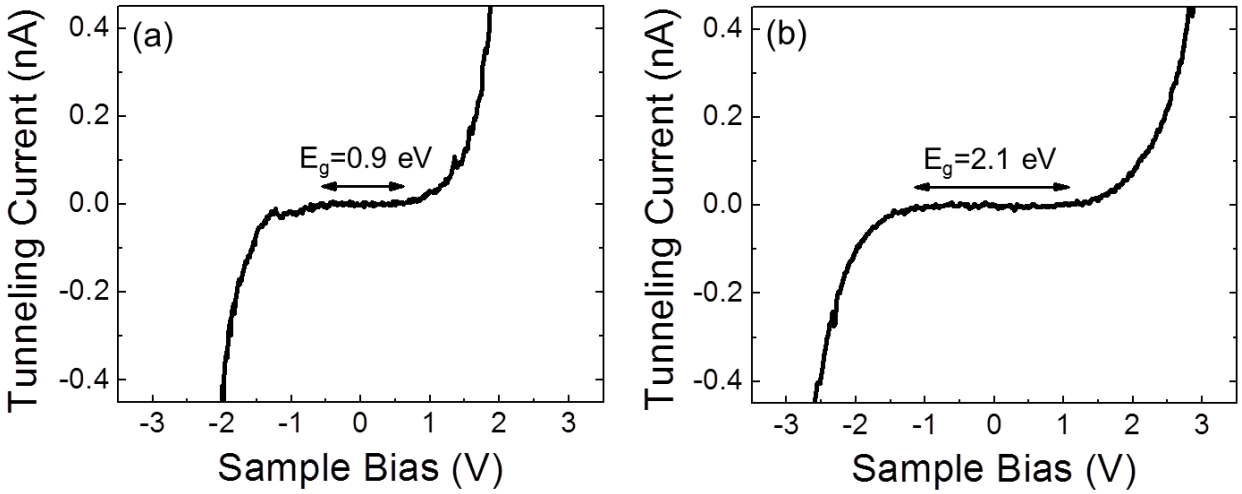

Figure S2: The tunneling current as a function of sample bias at room temperature on the LSMO/LAO (a) and LSMO/STO (b). This data was processed to obtain the dI/dV presented in Figure 4a in the paper.

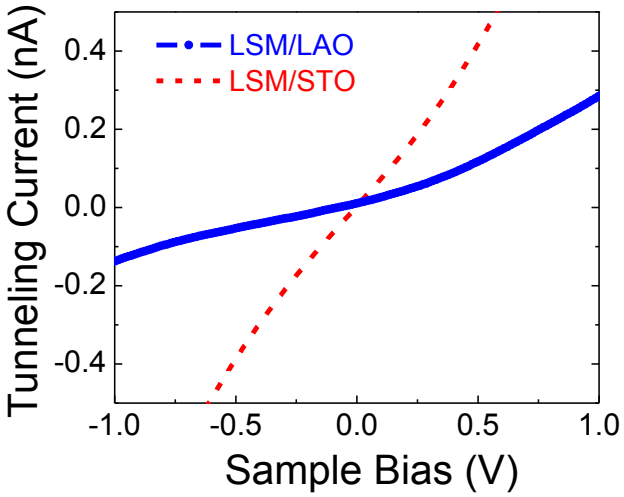

Figure S3: The tunneling current as a function of bias at high temperature (500 ^{o}C) on the LSMO/LAO (blue) and LSMO/STO (red). This data was processed to obtain the dI/dV presented in Figure 5c in the paper. Clearly the slopes of the (I/V) data near the Fermi level differ, such that it is higher for LSM/STO.

3) LSM model construction using DFT

To compare the strain-free concentration effects on the segregation, we have constructed two models, one with 25% (X_{Sr}=1/4) and another one 50% (X_{Sr}=1/2) Sr on A site on the surface. In addition, we also introduced a defect of oxygen vacancy into the X_{Sr}=1/2 model to understand how it would change the Sr segregation behavior. Surface segregation energy was calculated using Eq. (1).

$$E_{seg} = \frac{1}{2}\left\{\frac{1}{2}\left(E_{surf}(2x) + E_{surf}(0)\right) - E_{bulk}(x)\right\}, \qquad (1)$$

where E_{seg} is surface segregation energy per a Sr atom, E_{surf} the total energy of a slab with Sr atoms occupying La sites on a surface (i.e. top and bottom layer of the slab), E_{bulk} the total energy of a slab with Sr atoms occupying La sites in the bulk (i.e. central layer of the slab), x the number of Sr atoms in the unit cell.[4,5] Our model is schematically shown in Figure S4. For X_{Sr}=1/2, we put two Sr atoms into each top and bottom layer in the unit cell, while for X_{Sr}=1/4, we put one Sr atom into each top and bottom layer while remaining two Sr atoms in the central layer of the slab. The latter corresponds closely to our experimental observation in which Sr fraction on the surface (in bulk nominal) ~40% (30%). For both our models, Sr fraction on the total A sites is 20%. To represent the case that includes oxygen vacancy, we took out one oxygen atom from each top and bottom layer in the X_s=1/2 model. Oxygen vacancy formation energy was calculated as

$$E_{vac} = \frac{1}{2}\left\{E_{surf/bare} - \left(E_{surf/vac} + E_{O_2}\right)\right\}, \qquad (2)$$

where E_{vac} is oxygen vacancy formation energy, $E_{surf/bare}$ the total energy of a slab without vacancy, $E_{surf/vac}$ the total energy of a slab with vacancy, E_{O_2} the total energy of an isolated O_2 molecule.

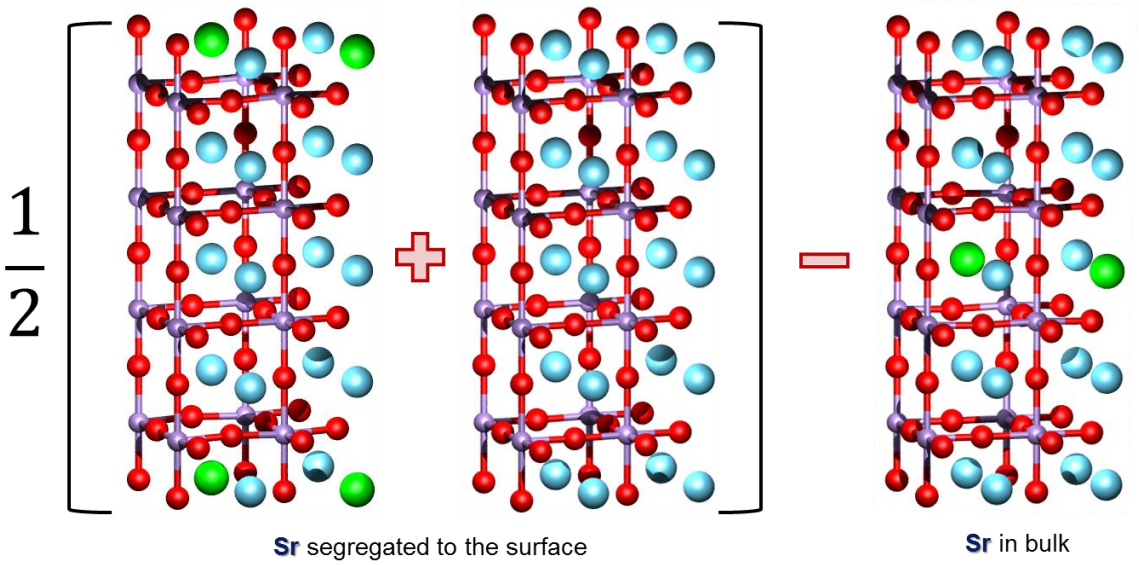

Figure S4: Schematic of the model and approach used to calculate the segregation energy per a Sr atom when X_{Sr}=1/2. For X_{Sr}=1/4, we substituted only one Sr atom on top and bottom surfaces with including two Sr atoms in the middle layer (not shown here). La atoms are shown as light blue spheres, Sr atoms as light green spheres, Mn atoms as purple spheres, O atoms as red spheres, respectively.

Our segregation energy values, shown in Figure 3a in the paper, are overestimated compared to the experimental observations from Herger et al.[6] and our own results (when we convert the Sr fraction on surface to the Sr segregation energy using the McLean model). At elevated temperatures, considering also the configurational entropy, less enhancement of Sr segregation on the surface is expected compared to the predictions made using only the enthalpic contributions at 0 K.[7,8] The temperature difference between our experiments and film synthesis at finite temperatures and our calculations at 0 K may therefore be the main cause of this quantitative inconsistency. As we mentioned in the paper, our experimental and theoretical results are, however, qualitatively in good agreement.

4) Total density of states calculations on LSM surfaces

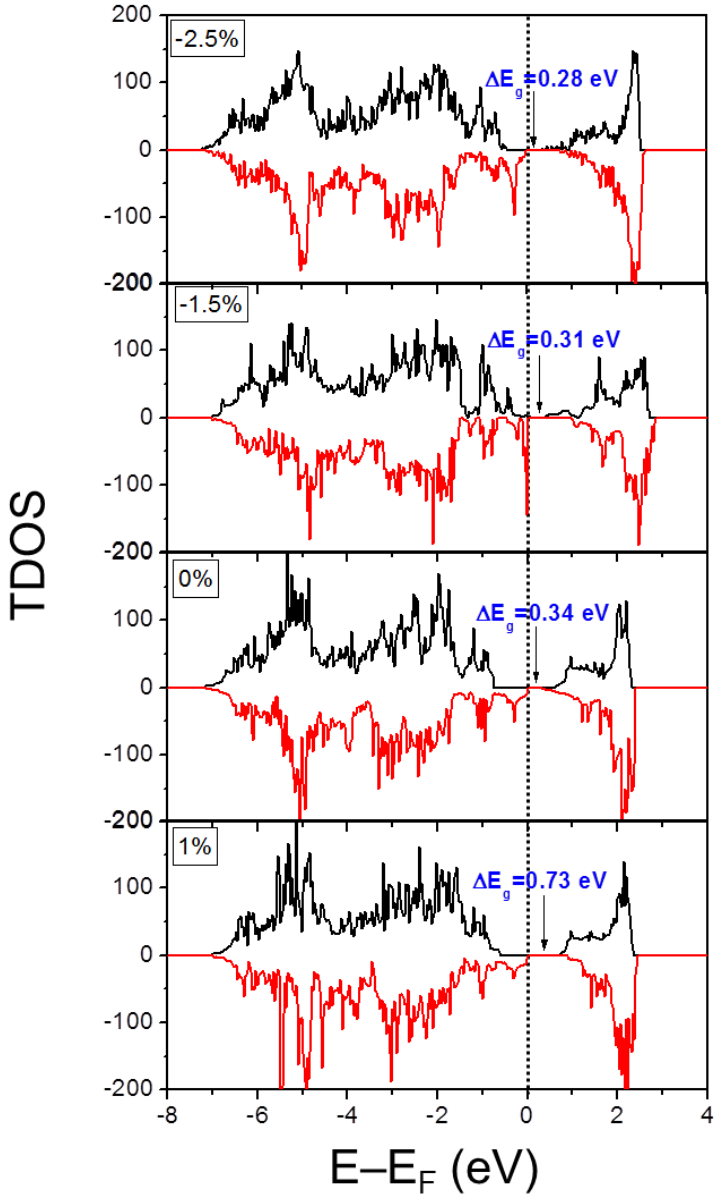

Figure S5: Total density of states of LSM(001) under four values of strain calculated from the X_s=1/2 model. The majority spin is shown as positive and the minority spin as negative. The zero of the energy scale is set to the Fermi level.

Our calculated DOS results are qualitatively consistent with Ma et al.'s recent DFT calculations at 0 K, in which the minority band gap in the half metallic character is slightly increased from the compressive to the tensile strain.[9]

References

(1) Lee, Y. P.; Park, S. Y.; Prokhorov, V. G.; Komashko, V. A.; Svetchnikov, V. L. Lattice-Strain-Driven Ferromagnetic Ordering in $La_{0.8}Sr_{0.2}MnO_3$ Thin Films. *Appl. Phys. Lett.* **2004**, *84*, 777-779.

(2) Satoh, I.; Kobayashi, T. Magnetoresistance of $La_{0.7}Sr_{0.3}MnO_3$ Thin Films Grown on Polycrystalline MgO Substrates. *Jpn. J. Appl. Phys.* **2001**, *40*, 586-591.
(3) *MTI Corporation*, *http://www.mtixtl.com*.
(4) Saul, A.; Weissmann, M. Magnetic Contribution to the Segregation Energies in Magnetic-Nonmagnetic Systems. *Phys. Rev. B* **1999**, *60*, 4982.
(5) Piskunov, S.; Heifets, E.; Jacob, T.; Kotomin, E. A.; Ellis, D. E.; Spohr, E. Electronic Structure and Thermodynamic Stability of $LaMnO_3$ and $La_{1-x}Sr_xMnO_3$ (001) Surfaces: Ab Initio Calculations. *Phys. Rev. B* **2008**, *78*, 121406/1-121406/4.
(6) Herger, R.; Willmott, P. R.; Schlepütz, C. M.; Björck, M.; Pauli, S. A.; Martoccia, D.; Patterson, B. D.; Kumah, D.; Clarke, R.; Yacoby, Y. *et al.* Structure Determination of Monolayer-By-Monolayer Grown $La_{1-x}Sr_xMnO_3$ Thin Films and the Onset of Magnetoresistance. *Phys. Rev. B* **2008**, *77*, 085401/1-085401/10.
(7) Fister, T. T.; Fong, D. D.; Eastman, J. A.; Baldo, P. M.; Highland, M. J.; Fuoss, P. H.; Balasubramaniam, K. R.; Meador, J. C.; Salvador, P. A. In Situ Characterization of Strontium Surface Segregation in Epitaxial $La_{0.7}Sr_{0.3}MnO_3$ Thin Films as a Function of Oxygen Partial Pressure. *Appl. Phys. Lett.* **2008**, *93*, 151904/1-151904/3.
(8) Sayle, T. X. T.; Parker, S. C.; Catlow, C. R. A. Surface Segregation of Metal Ions in Cerium Dioxide. *J. Phys. Chem.* **1994**, *98*, 13625-13630.
(9) Ma, C.; Yang, Z. Q.; Picozzi, S. Ab Initio Electronic and Magnetic Structure in $La_{0.66}Sr_{0.33}MnO_3$: Strain and Correlation Effects. *J. Phys. Condens. Matter*. **2006**, *18*, 7717-7728.